Characterization of low temperature deposited atomic layer deposition TiO_2 for MEMS applications

Yujian Huang,[a] Gregory Pandraud, and Pasqualina M. Sarro
DIMES (ECTM), Delft University of Technology, 2628 CT Delft, The Netherlands

(Received 3 September 2012; accepted 5 December 2012; published 26 December 2012)

TiO_2 is an interesting and promising material for micro-/nanoelectromechanical systems (MEMS/NEMS). For high performance and reliable MEMS/NEMS, optimization of the optical characteristics, mechanical stress, and especially surface smoothness of TiO_2 is required. To overcome the roughness issue of the TiO_2 films due to crystallization during deposition at high temperatures (above 250 °C), low temperature (80–120 °C) atomic layer deposition (ALD) is investigated. By lowering the deposition temperature, the surface roughness significantly decreases from 3.64 nm for the 300 °C deposited crystalline (anatase phase) TiO_2 to 0.24 nm for the 120 °C amorphous TiO_2. However, the layers deposited at low temperature present different physical behaviors comparing to the high temperature ones. The refractive index drops from 2.499 to 2.304 (at 633 nm) and the stress sharply decreases from 684 to 133 MPa. Superhydrophilic surface is obtained for the high temperature deposited TiO_2 under ultraviolet illumination, while little changes are found for the low temperature TiO_2. The authors demonstrate that by suitable postdeposition annealing, all the properties of the low temperature deposited films recover to that of the 300 °C deposited TiO_2, while the smooth surface profile (less than 1 nm roughness) is maintained. Finally, micromachining of the low temperature ALD TiO_2 by dry etching is also studied. © *2013 American Vacuum Society*. [http://dx.doi.org/10.1116/1.4772664]

I. INTRODUCTION

Recently, there has been a significant interest in using atomic layer deposition (ALD) materials in microelectromechanical systems (MEMS).[1–7] ALD is a deposition technique based on sequential surface reaction steps, where gaseous precursors are alternatively introduced into the chamber. Inert gases are purged into the chamber between each precursor pulse, resulting in a saturated chemisorption monolayer. Such self-limiting nature makes the deposited film highly conformal and provides excellent control over the film thickness. For MEMS applications, ALD coatings can be utilized to tune mechanical properties of moving parts by improving the wear and corrosion resistance,[1,2] can enhance the performance of biomaterials,[3] and can protect the devices from electrical shorts[4] and moisture-induced degradations.[5] ALD films can also serve as surface modification layers for better structural control in microfluidics[6] and higher sensing ability in chemical detections.[7]

Titanium oxide has been extensively studied for its high refractive index (RI or *n*), excellent optical transmittance and photocatalytic properties, its high capacitance and good insulating properties, its superhydrophilicity and biocompatibility.[8–10] TiO_2 films with large functional surface area have been obtained by depositing a thin TiO_2 layer coating on high-aspect-ratio nanostructures[11] or nanoparticles.[12] All these make TiO_2 a promising candidate for MEMS applications.

However, although the preferable crystalline anatase TiO_2 can be obtained by ALD, the roughness deriving from crystallization largely affects the performance of the device, for example, leads to signal loss[13] or device defects.[14] Thus, it is extremely important to reduce the roughness of ALD TiO_2 while maintaining the useful physical properties.

In this paper, ALD TiO_2 films with smooth surface are obtained by lowering the deposition temperature. The physical properties such as the surface morphology, the crystalline phases, the optical constants, the stress, and the wettability are examined and discussed for both of the as-deposited TiO_2 layers and the postdeposition annealed samples from a MEMS point of view. The micro-/nanomachining of ALD TiO_2 by dry etching is also explored.

II. EXPERIMENT

The deposition of ALD TiO_2 films was carried out in a commercial F120 thermal ALD reactor (ASM Microchemistry). The precursors were $TiCl_4$ and water, which were led into the reactor through solenoid valves. The alternating cycles of precursors were both 1 s, with purge cycles of N_2 in between (2 and 3 s after $TiCl_4$ and water, respectively). The reservoirs of the precursors were held at room temperature and the operation pressure was 1.5 Torr inside the chamber. Sample films were grown onto (100)-oriented Si substrates at temperatures ranging from 80 to 300 °C, with fixed 860 ALD cycles.

Some of the 120 °C deposited samples were subject to annealing in N_2 atmosphere at temperatures ranging from 150 to 600 °C. For annealing at 600 °C, the samples were loaded into a furnace at a standby temperature of 600 °C, with an N_2 flow of 3.0 slm. For annealing at lower temperatures, each of the samples was kept inside the ALD chamber after deposition with an N_2 flow of 500 sccm. The temperature was then ramped up to the expected value in 50 min for the subsequent annealing process.

[a]Electronic mail: yujian.huang@tudelft.nl

The surface roughness was analyzed with an AFM system (NT-MDT). The measurements were conducted in the semi-contact mode in air, with a scan rate of 0.5 Hz. The scanned size was $5 \times 5\,\mu m^2$ for the roughness calculation and $1 \times 1\,\mu m^2$ for grain size inspection. The crystallization form was examined by x-ray diffraction (XRD) recorded in a Bragg–Brentano geometry in a Bruker D5005 diffractometer. Data collection was carried out at room temperature using monochromatic Cu radiation ($K_{\alpha 1}$, $\lambda = 0.154056$ nm) with a step size of 0.038° 2θ and step time of 2 s. The optical properties of the TiO_2 films were determined with variable angle spectroscopic ellipsometry from J. A. Woollam. The analyzed spectral range was 245–1688 nm and the measurements were performed at incident angles of 55°–80° in 5° steps. The stress values were obtained using a TENCOR FLX 2908 system, by which the curvature changes of TiO_2 films on bare Si wafers were measured. The measurements were taken at room temperature. The static contact angles were measured on SCA20 type contact angle meter (Data-Physics). To enhance the hydrophilicity, samples were exposed to ultraviolet (UV) light with an OAI UV illuminator for 20 min–2 h. The repeatability test was carried out by storing the TiO_2 samples in dark for 12 h in between the UV illumination exposures.

Two reactive ion etching systems (SPTS Omega 201 etcher or Drytek 380 T etcher) were used to investigate the etch rate of the films. Commonly used plasma sources, such as SF_6, C_2F_6, CHF_3, Cl_2, and HBr based gas flows, were applied. Recipe details including etchants, gas flows, and radio frequency (RF) powers are listed in Table I. For comparison, other materials (Si, SiO_2, SiN_x, conventional photoresist: SPR3012 and ALD Al_2O_3) were also tested.

III. RESULTS AND DISCUSSION

A. Surface roughness and crystallization

In order to understand how the deposition temperature affects the crystallization and surface roughness, we first examined the surface morphology of ALD TiO_2 deposited from 300 °C down to 260 °C by AFM as shown in Fig. 1. The 300 °C deposited film was found to have an RMS value of 3.34 nm [Fig. 1(a)], with grain size of about 30 nm [Fig. 1(d)]. By lowering the deposition temperature in such range, the films remained quite rough. In fact, similarly high RMS values of 3.24 and 3.64 nm were obtained for the 280 and 260 °C films [Figs. 1(b) and 1(c)] and the grain size drastically increased to about 130 and 300 nm, respectively. Typical four folded crystalline TiO_2 grains can be recognized in the close-up AFM image in Fig. 1(e). Same tendency of the surface morphology change was reported by others.[15–17] The effect of nucleus density at the lower temperature is more pronounced than that of grain coalescence, thus causes the larger grain size.[17] On the other hand, much denser nuclei are formed at higher temperatures, which results in smaller grains. However, according to our RMS data, once crystallization happened during deposition, the roughness issue would exist even for the films with smaller grains.

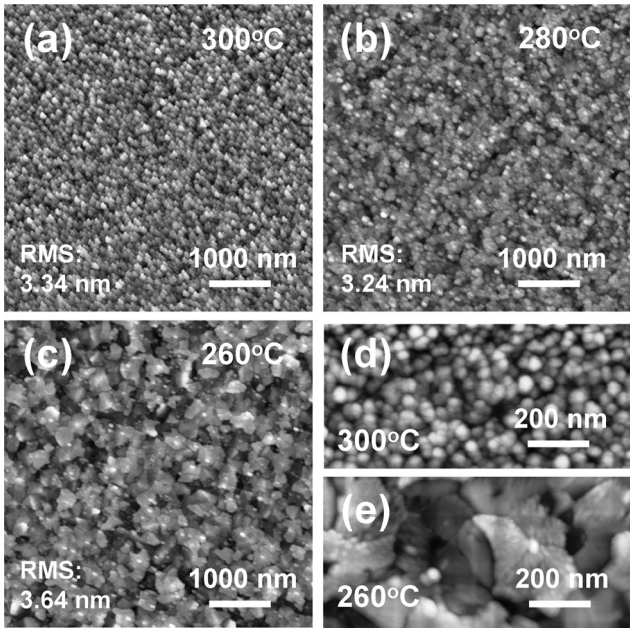

FIG. 1. AFM images of the surface morphology of ALD TiO_2 films deposited at (a) 300 °C, (b) 280 °C, and (c) 260 °C, together with grain size inspection of (d) the 300 °C sample and (e) the 260 °C sample.

By further lowering the deposition temperature, the surface morphology exhibited a different feature. A very smooth surface was obtained for the 120 °C deposited TiO_2 film, as shown in Fig. 2(a), with RMS of 0.24 nm. No crystalline grains were observed. It is well known that even though smooth and amorphous ALD TiO_2 can be obtained in thin films at temperature above 150 °C, crystallization, and thus roughness, occurs once it reaches certain cycle numbers.[16] However in this study, thicker film tests up to 3000 cycles still confirmed the smoothness and linear growth for the low temperature ALD TiO_2. Such superb smoothness even extended to the films after treatments like high temperature annealing. It is found out that the RMS value just slightly increased to 0.70 nm after 600 °C annealing for 4 h, which is significantly lower than that of the 300 °C as-deposited TiO_2 film.

The XRD patterns for the TiO_2 films grown at 300 and 120 °C are given in Fig. 3, together with the 600 °C annealed sample. Reported patterns of anatase TiO_2 (JCPDS No. 01-086-1157) are also labeled. The 300 °C film and the annealed film were found to be polycrystalline anatase, whereas the as-deposited 120 °C film was amorphous as indicated by its

TABLE I. Main parameters of the dry etching recipes.

Recipe	Flow (sccm)	Pressure (mTorr)	RF power (W)
C_2F_6 based[a]	65	130	250
CHF_3 based[a]	144	180	300
Cl_2 based[a]	100	160	160
HBr/SF_6[b]	40/20	10	15
SF_6/O_2[b]	20/20	50	50
SF_6 HP[b]	30	5	125

[a]In DryTek dry etching system.
[b]In Omega dry etching system.

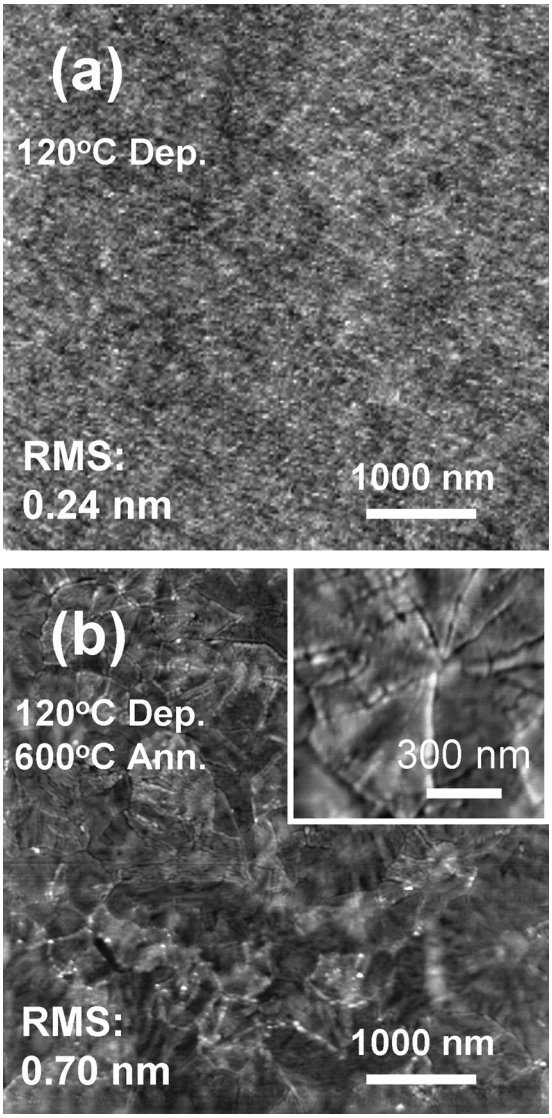

FIG. 2. AFM images of ALD TiO_2 films deposited at 120 °C: (a) as-deposited and (b) after annealing. A closeup of the recrystallized structure is shown in the inset.

featureless XRD spectra. No typical rutile peaks were seen even at this relatively high annealing temperature. Indeed, it is reported that no structural transformation to other crystalline phases of ALD TiO_2 for temperatures up to 700 °C in air and a sudden change to rutile happened at 750 °C.[18]

Considering the small roughness and the similar XRD pattern that the annealed TiO_2 has, smooth and high quality TiO_2 MEMS devices can thus be made by this "low temperature deposit and then anneal" method.

B. Deposition rate and optical properties

The optical properties and the thickness of the various ALD TiO_2 films were determined using spectroscopic ellipsometry. The absorption was fitted using a Gaussian oscillator model.[19] The optical constants and the film thickness can be deduced from the model. A Bruggeman type effective medium approximation (EMA) layer[20] was also adopted to represent the surface roughness. For the low temperature deposited samples, where roughness was not so significant, the EMA layer was fixed to a composition of 50% void and 50% of the underlying TiO_2 layer. For the crystallized samples, where grains were large enough to affect the roughness, such composition fraction was set as a variable in the fittings.

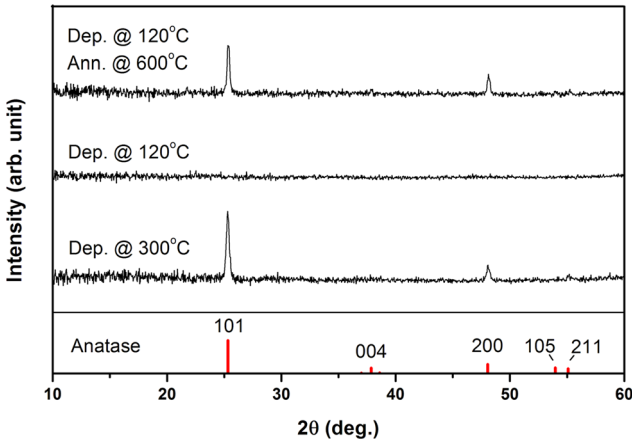

FIG. 3. (Color online) X-ray diffraction spectra of as-deposited and annealed ALD TiO_2 films. Diffraction peaks of anatase TiO_2 are also indicated.

Results and some of the fitting parameters of the ALD TiO_2 films are displayed in Table II. The thicknesses of EMA layer (d_{EMA}) were generally small (around 0.4 nm) for the low temperature samples and sharply increased to more than 2 nm for the high temperature samples, which is in good agreement with the AFM inspections. The fractions in the EMA layers of the high temperature TiO_2 films were found to slightly decrease with temperature. This can be explained by density change of the temperature-dependent nuclei discussed in Sec. III A. The total thickness was considered as the sum of d_{EMA} and the underneath continuous TiO_2 layer (d_{TiO_2}). Hence, the deposition rates of various ALD TiO_2 films were obtained as shown in Fig. 4. The total deposition rate at 300 °C was 0.52 Å/cycle and slightly increased to 0.53 Å/cycle for the 260 °C TiO_2. The trend is in good agreement to the results reported by Puurunen *et al.*,[21] in which a closely 1000-cycle number was used. Much more significant changes in growth rate were observed in the low temperature region, rising from 0.49 to 0.58 and 0.65 Å/cycle for 120, 100, and 80 °C TiO_2, respectively. Similar sharp increase of growth rate was also reported by

TABLE II. Thicknesses of ALD TiO_2 grown at different temperatures obtained by fitting the ellipsometry data with a Gaussian oscillator model, including an EMA layer.

T (°C)	d_{TiO_2} (nm)	d_{EMA} (nm)	TiO_2 fraction in EMA (%)	MSE	Total d (nm)
300	39.92	3.49	30.4	2.63	43.41
280	40.77	2.49	29	2.41	43.26
260	41.37	2.26	27.7	2.34	43.63
120	40.70	0.41	50	3.80	41.11
100	47.35	0.46	50	2.59	47.81
80	53.68	0.46	50	3.04	54.14

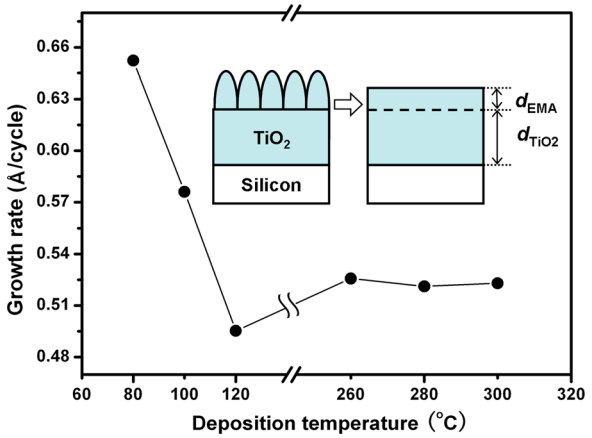

FIG. 4. (Color online) Growth rate of ALD TiO_2 films deposited at high and low temperatures. The model with an EMA layer representing the roughness is also schematically shown.

Aarik *et al.*[16] with deposition temperature varied from 150 to 100 °C. The O/Ti and the chlorine concentration at such low temperature range were studied by Aarik *et al.*[22] and Triani *et al.*[23] According to their results, calculated oxygen amount was sufficient to replace the chlorine ligands to form stoichiometric TiO_2; however, recorded chlorine concentration showed increasing ratio as the temperature decreased. This could mean that with low kinetic energy, some Ti–bonds are still occupied by chlorine, introducing point defects; at the same time instead of the tight Ti–O–Ti bonds, some looser Ti–O bonds are formed, enlarging the microstructures. Thus TiO_2 grows faster but with comparably mediocre properties.

The refractive indices of ALD TiO_2 layers deposited at temperatures from 80 to 300 °C are shown versus wavelength in Fig. 5. These refractive index curves can be categorized into two distinct groups: higher *n* for crystalline layers and lower *n* for amorphous layers. In each of these groups, the RI difference is very small. For example, considering the values at 633 nm (inset of Fig. 5), it gradually changes from 2.499 to 2.489 for temperatures from 300 to 260 °C, then sharply decreases to the range of 2.304–2.337 for temperatures from 120 to 80 °C. Thus, the crystalline form is critical for the refractive index value.

To obtain high refractive index values for such low temperature TiO_2 films, a 2-h postdeposition annealing at temperatures from 150 to 600 °C was carried out on the 120 °C deposited TiO_2 samples. The refractive index of these layers was determined using the same fitting model for the smooth films described above. As shown in Fig. 6, the *n* curves of TiO_2 annealed at 150 and 200 °C almost overlap with the as-deposited 120 °C curve, indicating that little recrystallization happened in this anneal temperature range. Significant change was found at annealing temperatures above 200 °C, leading to a gradual refractive index rebound to high values. For example, *n* at 633 nm increased from 2.339 to 2.368, 2.393, and 2.434 for the 150, 300, 400, and 600 °C annealed samples, respectively. According to our XRD results, clear anatase phases were found in the 600 °C annealed film. Thus, postdeposition annealing at relatively high temperature for short time can be an effective way to regain high optical properties. Another way for recrystallization is to increase the annealing time at a relatively low temperature. For example, Yuwono *et al.*[24] reported that amorphous TiO_2 grown by sol-gel could turn into anatase by annealing at 150 °C for 24 h.

By carefully examining the refractive index peaks of all the tested samples, an additional small pike can be observed for each of the crystallized samples at the wavelength of around 300 nm and the shifting of the peak positions was also noticed. In order to understand such evolution, the spectra of their extinction coefficient (*k*) were plotted in Fig. 7. The *k* curves of the 300 °C deposited TiO_2 showed two explicit peaks at about 3.96 and 4.56 eV, which were identical to the bulk anatase.[25] On contrary, a much smoother saturated ramp, instead of any clear peaks, could be found for the 120 °C deposited amorphous TiO_2. Therefore, it could be concluded that the shapes and positions of the corresponding

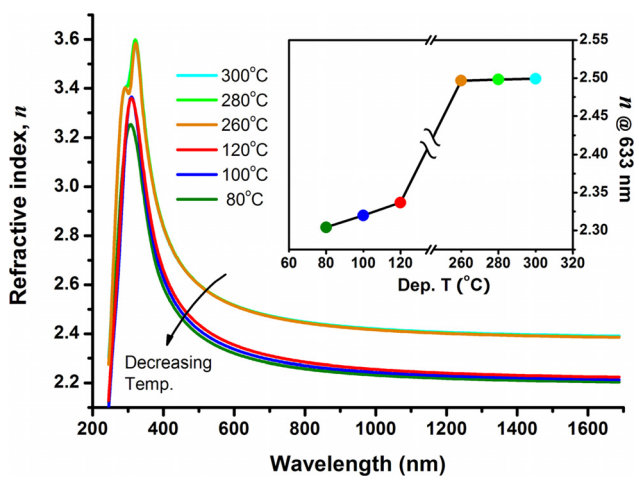

FIG. 5. (Color online) Refractive index spectra of ALD TiO_2 films deposited at temperatures between 300 and 80 °C obtained by spectroscopic ellipsometry. The inset shows the values at 633 nm.

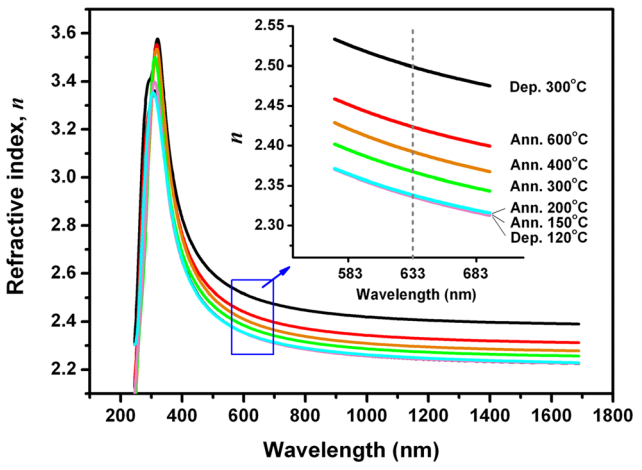

FIG. 6. (Color online) Recovering of refractive index for the 120 °C deposited samples by annealing. The annealing temperature ranges from 150 to 600 °C. For comparison, RI curves of the as-deposited 120 and 300 °C ALD TiO_2 films are also plotted.

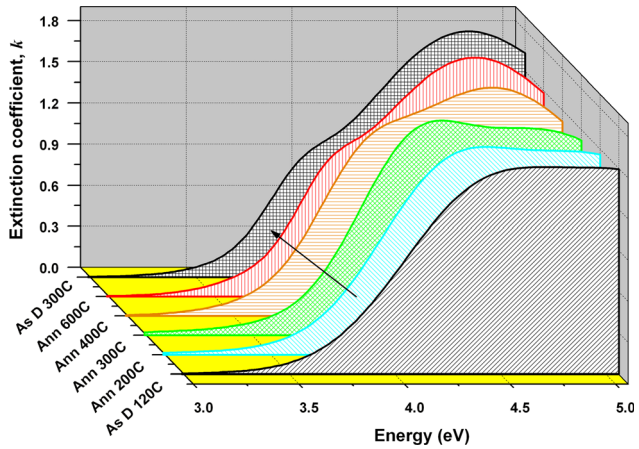

FIG. 7. (Color online) Extinction coefficient spectra of different ALD TiO_2 films. Samples from bottom to top: as deposit at 120 °C; 120 °C deposited and annealed at 200, 300, 400, and 600 °C; as deposit at 300 °C.

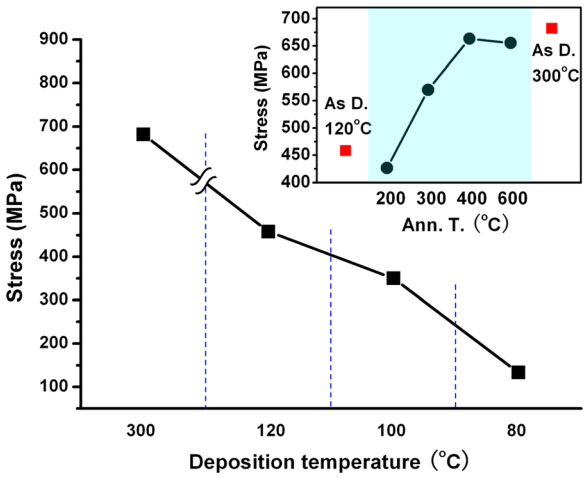

FIG. 8. (Color online) Relationship between the stress of ALD TiO_2 layers and their deposition temperature. The inset shows the effect of annealing on the stress of the 120 °C layers.

refractive index curves differentiated with the crystalline phase.

The evolution of the k curve was interesting by changing the annealing temperature of the 120 °C deposited TiO_2 samples, as shown in Fig. 7. At annealing temperatures less than 200 °C, little change was observed along the spectra, which was in good agreement with the observation of refractive index that little change occurred. Once the temperature reached 300 °C, a bump could be found at around 4.35 eV with the k curve. Such small peak declined toward lower energy level as the annealing temperature increased. In addition, another larger peak emerged at higher energy level above 4.5 eV at temperatures higher than 400 °C. With these changes, the shape of the 600 °C annealed k curve was already quite close to the 300 °C deposited TiO_2. Since the changes were in good agreement of the XRD results, the optical constants can also be the indicator of crystalline phases.

C. Stress

Stress is an important factor for MEMS devices consisting of moving mechanical parts. In our case, all of the studied ALD TiO_2 samples presented tensile stress (see Fig. 8), which would benefit membrane fabrications for MEMS devices.[26] The stress values decreased with decreasing the deposition temperature. High stress of 682 MPa was obtained for the 300 °C deposited ALD TiO_2 films. A significant stress decline was found in the low temperature region, i.e., from 458 MPa at 120 °C to a remarkably low value of 133 MPa at 80 °C. This is probably attributed to the much looser Ti–O bonds at lower temperature.

To examine the annealing effect on stress, a 2-h annealing treatment on the 120 °C grown ALD TiO_2 samples was carried out at temperatures of 200, 300, 400, and 600 °C. As shown in the inset of Fig. 8, the stress value slightly decreased to 426 MPa for 200 °C annealing and experienced a large rebound to 560 MPa for the 300 °C annealing. For annealing temperatures above 400 °C, the stress value reached about 660 MPa, a value similar to that of the as-deposited 300 °C TiO_2. As also indicated by the optical analysis reported above, notable changes were found for annealing temperatures above 200 °C, while almost no effect was observed for temperatures below 200 °C. Thus, the recrystallization is believed to be the main cause for the stress changes.

D. Wettability

Wettability is another important property for MEMS applications, especially for microfluidic systems or biosensing devices. As shown in Fig. 9, all of the ALD TiO_2 films had superhydrophilic surfaces when taking out from the deposition chamber. This can be explained by the ALD mechanism and the precursors used.[27] In the very last step of ALD of TiO_2, the surface of the film is terminated with the OH– groups from the water precursor, which are responsible for the hydrophilicity. The films gradually became hydrophobic when stored in dark atmosphere. After about 90 days, they all presented hydrophobic surfaces with a water contact angle of 70°–80°. This could mean that the Ti–OH bond is not so stable and might be replaced by Ti–O–Ti to the adjacent Ti atom.

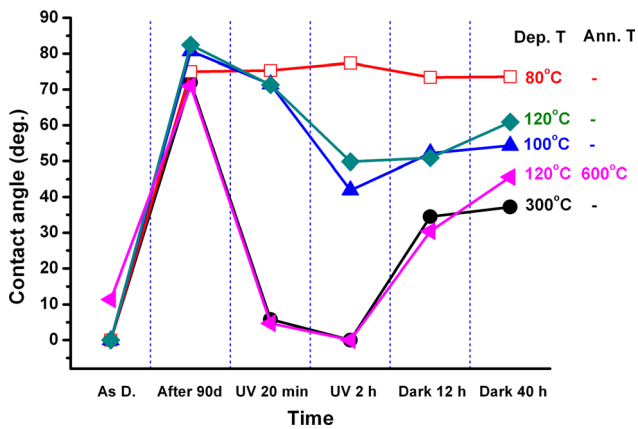

FIG. 9. (Color online) Evolution of water contact angles of different ALD TiO_2 films vs storage time and UV illumination.

To examine the UV-induced wettability conversion, two steps of UV illumination were implemented. The first one lasted for 20 min and the second one lasted for 2 h. The water contact angles were measured immediately after these two illumination steps. The 300 °C deposited TiO_2 rapidly became hydrophilic (contact angle of about 5°) after the first UV step, while a smaller reduction of the contact angle was obtained for samples deposited at 100 and 120 °C. The 80 °C TiO_2 showed an unobvious opposite tendency, as it became a little bit more hydrophobic after the UV illumination.

The anatase TiO_2 samples behaved superhydrophilic after the second longer UV illumination step, with contact angles almost equal to 0°. According to Wang *et al.*,[28] this effect was due to the production of oxygen vacancies formed by the UV-induced Ti states change. The oxygen vacancies strongly interact with water thus OH− groups occupy such vacancies and the surface becomes hydrophilic. The 100 and 120 °C samples also experienced a deeper contact angle decrease after 2-h UV illumination, but not yet to reach the hydrophilic state. This may be caused by the presence of nanocrystallites in a limited amount in such low temperature TiO_2 films so that insufficient UV-induced oxygen vacancies were formed. The deposition temperature is critical for the amount of such crystallites. This can be proved by the larger contact angle dip of the 120 °C film compared to the 100 °C film. Similar to the first UV step, the contact angle of the 80 °C TiO_2 increased slightly.

The samples were then kept in air and dark environment for 12 h. For the crystalline TiO_2 films, the contact angles increased to more than 30°. This change was significantly faster than that in the first stage when films were stored for 90 days after deposition (little changes were found in the first few days). All the amorphous films, except for the 80 °C TiO_2, experienced similar but smaller contact angle rebound after 12 h. Further storing in dark environment resulted in more hydrophobic films.

It is useful to find that the annealed film presented almost the same wettability with the 300 °C deposited TiO_2 film. To examine the validity and repeatability of such annealed film, hydrophilic/hydrophobic conversion was also tested. Good consistency was found, as illustrated in Fig. 10(a). After every UV illumination, the sample presented superhydrophilic surface and then bounced to about 30° when stored in the dark for 12 h. Representative contact angle images are also shown in Figs. 10(b) and 10(c).

To clarify the effect of organics/water in such hydrophilic/hydrophobic transition, equivalent experiments in vacuum and air were carried out (see Fig. 11). The first step was tests for hydrophobic surfaces undergoing UV illumination. After 90 days of storage, the anatase ALD TiO_2 samples performed relatively hydrophobic surfaces with contact angles in the range of 70°–73°. In order to eliminate the possible effect from absorbed organics, one of the samples was cleaned in 99% HNO_3 for 10 min and rinsed in deionized water for 10 min. After drying, it was placed in a vacuum chamber for 5 min to allow vacuum stability and desorption of H_2O molecules on the surface. An UV light source outside the chamber was then switched on and projected through a quartz window onto the TiO_2 sample. Little change of contact angle was found after 1-h UV illumination. The surface remained hydrophobic. However, by immediately undergoing the UV illumination in air, it presented rapid conversion into superhydrophilic, which was similar to the control samples that did not experience the 99% HNO_3 cleaning and vacuum treatments. The contact angle after 1-h UV illumination was 3.1°. This suggests that additional compounds, maybe either organics or water, even in small amount, are needed for the UV induced transition.

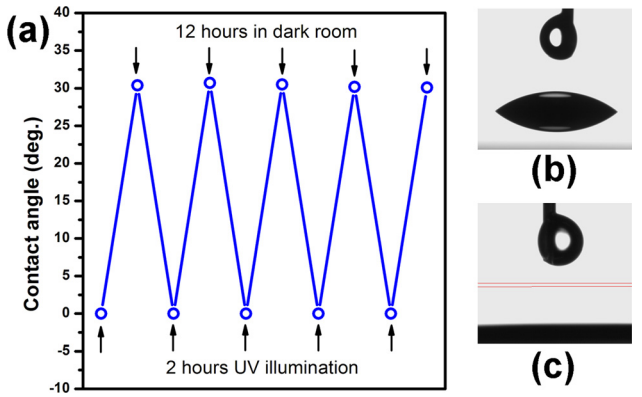

FIG. 10. (Color online) (a) Reversion of wettability of the 600 °C annealed sample under alternate UV illumination and storage in dark environment. [(b) and (c)] Representative photos of water drops in contact angle measurement.

On the other hand, as proven by the second step tests in dark storage, vacuum can help the regaining of hydrophobicity in much shorter time. According to Fig. 11, when stored in vacuum, the contact angle of a superhydrophilic TiO_2 surface rapidly bounded back to 63.5° in 12 h, while the control sample, kept in air, only showed 34.5° after the same time. Moreover, it took the control sample several days to recover back to more than 60°. The faster hydrophobicity change is probably due to the accelerated loss of the absorbed molecules and the quick restoration from OH-terminated surface by vacuum. Like the above-mentioned UV induced transition, more studies are required to fully understand the mechanism.

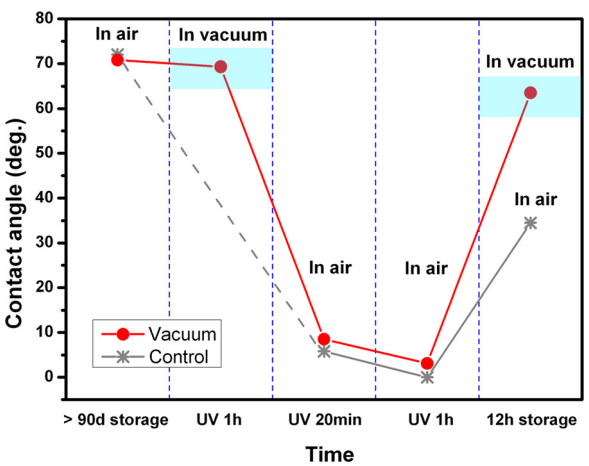

FIG. 11. (Color online) Comparison of water contact angles of samples treated in vacuum and in air.

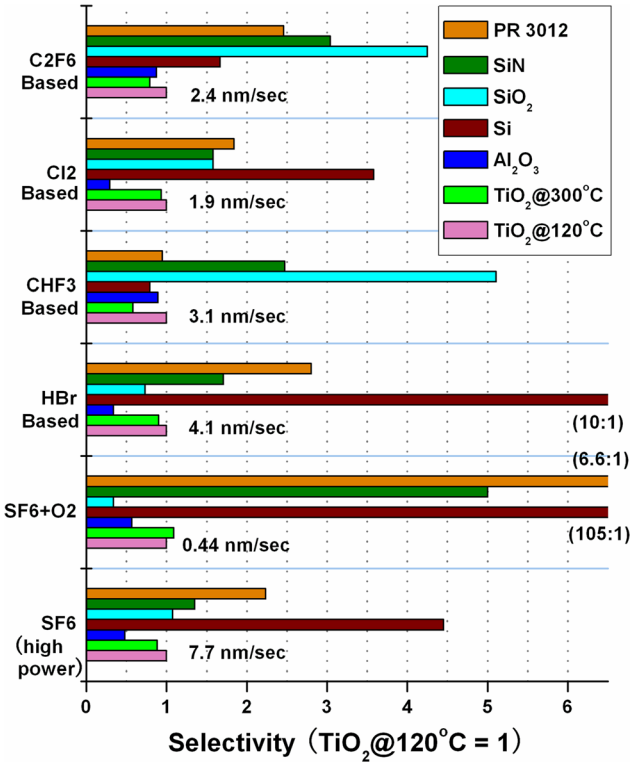

FIG. 12. (Color online) Etch rate diagram of ALD TiO_2. The selectivity of frequently used materials, defined as the ratio of the etch rates of the materials over the etch rate of the 120 °C deposited TiO_2, is plotted for different plasma etchants and conditions. The etch rate of the 120 °C deposited TiO_2 is listed next to the each corresponding recipe group.

E. Etch rates in plasma etching

Another important characterization of these layers is related to the dry etching as this is relevant for precise anisotropic micro-/nanomachining of TiO_2 or in contrast, to use it as protective coatings. The etch rates of ALD TiO_2 deposited at 120 °C in different etching schemes are listed in Fig. 12. The etch rates of other commonly used materials for MEMS fabrication are measured and compared in order to identify the suitable masking layer for accurate patterning of TiO_2. Generally speaking, ALD TiO_2 is a very hard-to-etch material. It has a strong resistance to most of the etchants (etch rate < 1 nm/s) in low RF power conditions, except for the HBr/SF_6 recipe (4.1 nm/s). By increasing the RF power, the etch rates increased (in the range of 1.9–7.7 nm/s). Similar resistant-to-etchant behaviors were found for TiO_2 deposited at different temperatures, with slightly increased etch rates for the amorphous low temperature TiO_2.

For TiO_2 deposited at 120 °C, the highest etch rate (7.7 nm/s) was observed in the high power SF_6 etching which produced a strong mechanical bombardment. However, long time in such high power etching could lead to damaged surfaces and affect uniformity. Because of the bombardment-dominated principle, similar etch rates were measured for SiO_2, SiN_x, and TiO_2. Only Al_2O_3 showed a smaller etch rate (3.7 nm/s). Comparing to other etchants, the mixture of HBr and SF_6 can improve the etch rate of TiO_2, even with low RF power. However, similar to other recipes, the key issue is the poor selectivity to shape TiO_2. Thus, it is hard to find a suitable mask material for patterning TiO_2. To circumvent this problem, novel nanofabrication techniques are necessary for high-aspect-ratio TiO_2 nanostructure fabrications.

On the other hand, TiO_2 can be considered as an excellent masking or protective coating material. Selectivity of more than three over low temperature ALD TiO_2 was found for SiO_2 (4.3) and SiN (3.1) with C_2F_6 based recipe, for SiO_2 (5.1) with CHF_3 based recipe, and for Si (3.6) with Cl_2 based recipe, respectively. In particular, selectivity of Si over TiO_2 was found over 10:1 for HBr/SF_6 recipe and more than 100:1 for SF_6/O_2 based recipe. As TiO_2 is also highly resistant to a lot of wet etchants[10,29] and the dense ALD coatings[30] can effectively decrease gas or liquid penetrations, low temperature ALD TiO_2 is a promising passivation material for MEMS devices.

IV. CONCLUSIONS

Improvement of surface smoothness of ALD TiO_2 thin films, while keeping the high functional quality, is achieved by lowering the deposition temperature to 80–120 °C and defining suitable postdeposition annealing. Some important properties such as surface morphology, crystallization phases, growth rates, and optical constants are characterized. Key performances and issues for MEMS applications, including stress, wettability conversion, and micromachining by dry etching, are also addressed. Annealing at temperatures above 200 °C can turn such low temperature deposited films from amorphous to anatase with less than 1 nm roughness. These findings indicate that smooth TiO_2-based MEMS devices with excellent optical and mechanical properties can be realized.

ACKNOWLEDGMENTS

The authors gratefully acknowledge the DIMES IC Process Group TU Delft, for technical supports and Ruud Hendrikx at the Department of Materials Science and Engineering of TU Delft for the x-ray analysis. This work was supported by TFN program of the Dutch Technology Foundation STW (Project 10026).

[1]T. M. Mayer, J. W. Elam, S. M. George, P. G. Kotula, and R. S. Goeke, Appl. Phys. Lett. **82**, 2883 (2003).
[2]T. W. Scharf, S. V. Prasad, M. T. Dugger, P. G. Kotula, R. S. Goeke, and R. K. Grubbs, Acta Mater. **54**, 4731 (2006).
[3]S.-M. Lee, E. Pippel, U. Gösele, C. Dresbach, Y. Qin, C. V. Chandran, T. Bräuniger, G. Hause, and M. Knez, Science **324**, 488 (2009).
[4]N. D. Hoivik, J. W. Elam, R. J. Linderman, V. M. Bright, S. M. George, and Y. C. Lee, Sens. Actuators, A **103**, 100 (2003).
[5]E. Langereis, M. Creatore, S. B. S. Heil, M. C. M. van de Sanden, and W. M. M. Kessels, Appl. Phys. Lett. **89**, 081915 (2006).
[6]D. Losic, G. Triani, P. J. Evans, A. Atanacio, J. G. Mitchell, and N. H. Voelcker, J. Mater. Chem. **16**, 4029 (2006).
[7]X. Zhang, J. Zhao, A. V. Whitney, J. W. Elam, and R. P. Van Duyne, J. Am. Chem. Soc. **128**, 10304 (2006).
[8]X. Chen and S. S. Mao, Chem. Rev. **107**, 2891 (2007).
[9]U. Diebold, Surf. Sci. Rep. **48**, 53 (2003).
[10]R. L. Puurunen, J. Saarilahti, and H. Kattelus, ECS Trans. **11**, 3 (2007).
[11]J. W. Elam, D. Routkevitch, P. P. Mardilovich, and S. M. George, Chem. Mater. **15**, 3507 (2003).
[12]S. D. Standridge, G. C. Schatz, and J. T. Hupp, Langmuir **25**, 2596 (2009).

[13]J. Aarik, A. Aidla, A.-A. Kiisler, T. Uustare, and V. Sammelselg, Thin Solid Films **305**, 270 (1997).
[14]N. Gaillard, L. Pinzelli, M. Gros-Jean, and A. Bsiesy, Appl. Phys. Lett. **89**, 133506 (2006).
[15]D. R. G. Mitchell, D. J. Attard, and G. Triani, Thin Solid Films **441**, 85 (2003).
[16]J. Aarik, A. Aidla, H. Mändar, T. Uustare, M. Schuisky, and A. Hårsta, J. Cryst. Growth **242**, 189 (2002).
[17]H.-E. Cheng and C.-C. Chen, J. Electrochem. Soc. **155**, D604 (2008).
[18]A. Niilisk, M. Moppel, M. Pärs, I. Sildos, T. Jantson, T. Avarmaa, R. Jaaniso, and J. Aarik, Cent. Eur. J. Phys. **4**, 105 (2006).
[19]D. De Sousa Meneses, M. Malki, and P. Echegut, J. Non-Cryst. Solids **352**, 769 (2006).
[20]D. E. Aspnes, Thin Solid Films **89**, 249 (1982).
[21]R. L. Puurunen, T. Sajavaara, E. Santala, V. Miikkulainen, T. Saukkonen, M. Laitinen, and M. Leskelä, J. Nanosci. Technol. **11**, 8101 (2011).
[22]J. Aarik, A. Aidla, H. Mändar, and T. Uustare, Appl. Surf. Sci. **172**, 148 (2001).
[23]G. Triani, J. A. Campbell, P. J. Evans, J. Davis, B. A. Latella, and R. P. Burford, Thin Solid Films **518**, 3182 (2010).
[24]A. H. Yuwono, B. Liu, J. Xue, J. Wang, H. I. Elim, W. Ji, Y. Li, and T. J. White, J. Mater. Chem. **14**, 2978 (2004).
[25]J. G. E. Jellison, L. A. Boatner, J. D. Budai, B. S. Jeong, and D. P. Norton, J. Appl. Phys. **93**, 9537 (2003).
[26]P. J. French, P. M. Sarro, R. Malléeb, E. J. M. Fakkeldij, and R. F. Wolffenbuttel, Sens. Actuators, A **58**, 149 (1997).
[27]R. L. Puurunen, J. Appl. Phys. **97**, 121301 (2005).
[28]R. Wang, K. Hashimoto, A. Fujishima, M. Chikuni, E. Kojima, A. Kitamura, M. Shimohigoshi, and T. Watanabe, Nature **388**, 431 (1997).
[29]B. S. Richards, Prog. Photovoltaics **12**, 253 (2004).
[30]M. D. Groner, F. H. Fabreguette, J. W. Elam, and S. M. George, Chem. Mater. **16**, 639 (2004).